Accepted for Publication in Physical Review Materials

Converse Magneto-Electric Effects in Composites of Liquid Phase Epitaxy Grown Nickel Zinc Ferrite Films and Lead Zirconate Titanate: Studies on the Influence of Ferrite Film Parameters

Peng Zhou,[1,2] M. A. Popov,[1,3] Ying Liu, [1,2] Rao Bidthanapally,[1] D. A. Filippov,[4] Tianjin Zhang,[2 a)] Yajun Qi,[2] P. J. Shah,[5] B. M. Howe,[5] M. E. McConney,[5] Yongming Luo,[6] G. Sreenivasulu,[7] G. Srinivasan, [1,5 b)] and M. R. Page[5, c)]

[1] Physics Department, Oakland University, Rochester, MI 48309, USA
[2] Department of Materials Science and Engineering, Hubei University, Wuhan 430062, China
[3] Faculty of Radiophysics, Electronics and Computer Systems, Taras Shevchenko National University of Kyiv, Kyiv, 01601, Ukraine
[4] Novgorod State University, Veliky Novgorod, 173003 Russia
[5] Materials and Manufacturing Directorate, Air Force Research Laboratory, Wright-Patterson Air Force Base, Dayton, OH 45433, USA
[6] Materials Science Division, Argonne National Laboratory, Argonne, Illinois 60439, USA
[7] Department of Materials Science and Engineering, Virginia Tech, Blacksburg, VA 24060, USA

Abstract

The interactions between electric and magnetic subsystems in a ferroelectric-ferromagnetic composite occur through mechanical forces. Here we discuss results of a systematic investigation on the strength of the magnetic response of the composite to an applied electric field, known as the converse magneto-electric (CME) effect, and its dependence on the ferroic order parameters and volume fraction for the two phases. Studies were carried out on composites of lead zirconate titanate (PZT) and 2-30 micron thick nickel zinc ferrite (NZFO) films grown by liquid phase epitaxy (LPE) on lattice matched (100) and (111) MgO substrates. Ferromagnetic resonance (FMR) was utilized to

determine the strength of CME from data on electric field E induced shift in the resonance frequency and its dependence on ferrite film orientation and thickness as well as MgO substrate thickness. The CME coupling coefficient *A* was found to be a factor of two to four higher in samples with NZFO films with (100) orientation than for (111) films. A decrease in *A* was measured with increasing ferrite film thickness and a very significant enhancement in the strength of CME was measured for decreasing MgO thickness. A model for CME that takes into consideration the influence of non-ferrroic MgO substrate was developed and estimated *A*-values are in very good agreement with the data. The results presented here are also of importance for a new class of electric field tunable ferrite microwave devices.

Authors to whom correspondence should be addressed:

[a] *zhangtj@hubu.edu.cn*; [b] *srinivas@oakland.edu*; [c] *michael.page.16@us.af.mil*

1. Introduction

Multiferroic composites with ferromagnetic and ferroelectric phases show coupling between the magnetic and electric subsystems that is attributed to mechanical strain produced in a magnetic and/or electric field [1-5]. There are two types of magneto-electric (ME) coupling which is a product-property [6,7]. In the case of direct-ME (DME) interaction, magnetostrictive strain in the ferromagnetic phase in a magnetic field is transferred to the ferroelectric phase and is measured as variations in the ferroelectric order parameter such as polarization and permittivity [8-10]. The magnetic response of the composite to an applied electric field, termed converse ME effect (CME) occurs due to piezoelectric strain in the ferroelectric phase that manifests as a change in the magnetization or anisotropy field [11-14]. Several composites with ferromagnetic metals, alloys or oxides and ferroelectric barium titanate (BTO), lead zirconate titanate (PZT) or lead magnesium niobate-lead titanate (PMN-PT) were reported to show strong ME coupling [3]. The ME phenomena are also of importance for novel magnetic sensors, tunable radio-frequency devices and power electronics [3,15].

This report is on converse-ME effects in composites of spinel ferrites and PZT that are of fundamental and technological importance. The strength of CME, in general, is determined by ferromagnetic resonance (FMR) measurements when the composite is subjected to an electric field E or by measuring magnetization M versus magnetic field H under E [16-18]. In the case of FMR, E-induced shift in the resonance field δH_r or frequency δf_r is measured to determine the CME coupling constant $A = \delta H_r/E$ (or $\delta f_r/E$). A giant CME was reported in FeGaB/ferroelectric composites [19]. The nature of CME in

composites with ferrimagnetic oxides such as yttrium iron garnet and spinel or hexagonal ferrites has been studied extensively in recent years [19-23]. Coupling strengths A = 1 to 10 MHz cm/kV were reported for composites of epoxy or eutectic bonded yttrium iron garnet (YIG), nickel ferrite, or hexaferrites with PZT or PMN-PT [3]. Heterostructures of nickel ferrite and PMN-PT prepared by chemical vapor deposition were also reported to show strong CME effects [20].

The CME in ferrite-ferroelectric composites are of particular interests due to their potential for dual H- and E-tunable ferrite devices [24]. Ferrites are materials of choice for use in FMR-based high frequency signal processing devices such as resonators and filters due to their desirable characteristics including low-losses. A key disadvantage for their use in broad-band devices, however, is the need for a variable magnetic field that could only be produced by a solenoid. The magnetic tuning in general is slow, noisy and requires very high power. An attractive alternative to H- tuning is the electric field or voltage tuning that can be accomplished with the use of a ferrite-ferroelectric composite and the tuning will be fast, passive and the devices can be miniaturized and integrated with semiconductor devices.

Here we discuss results of a systematic study on the converse-ME effects by E-tuning of FMR in composites of PZT and nickel zinc ferrite (NZFO) films grown by liquid phase epitaxy (LPE). According to models, the ME coefficient A is a function of thickness (or volume) for the ferrite and PZT and is directly proportional to the product of magnetostriction λ for the ferrite and piezoelectric coefficient d for PZT and inversely proportional to the saturation magnetization M_s [25,26]. We choose spinel ferrite with the composition $Ni_{0.8}Zn_{0.2}Fe_2O_4$ since it has the highest λ-value amongst NiZn-ferrites [27].

Films were grown on (111) and (100) substrates of MgO to investigate the crystallographic orientation dependence of λ and, therefore, A. Ferrite films with a series of thickness ranging from 2 to 30 μm were grown by LPE for studies on t-dependence of A. LPE is ideally suitable for growth of such thick films free of defects so that the FMR line-width is small enough for accurate measurements of shift in resonance field/frequency [28-30]. Measurements were done for static fields E and H along either [111] for films on (111) MgO and along [100] for films on (100) MgO. Important findings are as follows: (i) ME coupling coefficient A shows a linear decrease with increasing ferrite film thickness; (ii) Composites with (100) NZFO show a much higher A-value than for (111) NZFO; (iii) A significant increase in the strength of CME was measured when the substrate thickness was decreased from 0.5 mm to 0.2 mm; and (iv) The measured A-values compare favorably with estimated values. Details of the ferrite film synthesis, results on measurements of FMR under an electric field, and estimation of A are provided in the following sections.

2. Growth of Nickel Zinc Ferrite Films by Liquid Phase Epitaxy

The LPE technique is ideally suitable for the growth of single crystal films of ferrites and garnets on lattice matched substrates [27-30]. Past efforts in this regard include growth of YIG films on gadolinium gallium garnet (GGG) substrate and spinel ferrite films on MgO and $MgAl_2O_4$ substrates. In this study films of NZFO were grown by LPE on (111) and (100) substrates of MgO which has a cubic structure with the lattice constant $2a_0$ = 0.8424 nm. For NZFO spinel ferrite films with a_0 = 0.8357 nm the expected substrate-to-film lattice mismatch is 0.78 % and is small enough for LPE growth of good quality films. The

thickness of (111) MgO substrates was 0.5 mm while (100) MgO substrates were either 0.5 mm thick or 0.2 mm thick. We employed the LPE technique to grow the films under isothermal conditions from super-cooled melts consisting of PbO-B_2O_3 flux and ferrite components NiO, ZnO and Fe_2O_3. Ultrahigh purity chemicals were dry-mixed and placed in a Pt-crucible. The amount of chemicals used in molar percentage is listed in Table 1 and are for nominal composition of $Ni_{0.8}Zn_{0.2}Fe_2O_4$ [30]. The key parameters for the flux used for the growth are the molar ratios of PbO/B_2O_3 = 15.4, Fe_2O_3/(NiO + ZnO) = 10.455, and ferrite/(PbO+B_2O_3) = 0.095.

Table 1: Composition of the flux in molar percentage used for the growth of nickel zinc ferrite films by LPE. Tg is the growth temperature.

	Original flux	Modified flux
PbO	85.1	84.95
B_2O_3	5.48	5.47
Fe_2O_3	8.7	8.68
NiO	0.67	0.67
ZnO	0.16	0.23
Tg	780-810°C	780-810°C

A vertical split-furnace, as shown in Fig.1(a), with a constant temperature zone of 6 cm was used for this purpose. The Pt-crucible with the oxides was placed in the uniform temperature zone and heated to 1075°C. The flux with crystal components was homogenized for 8-10 hours at this temperature and then cooled slowly to the growth temperature T_g = 780-810 °C at the rate of 1°C/min. MgO substrates held on platinum wires, in the vertical plane, were

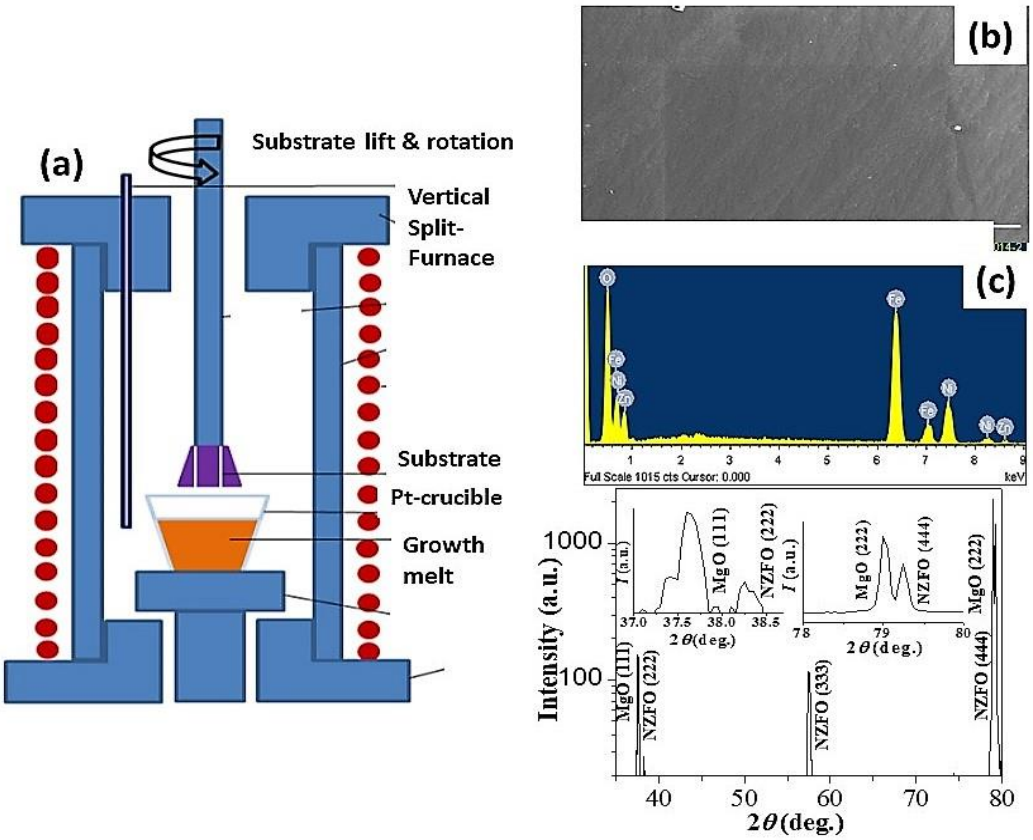

Fig.1

Fig.1. (a) Schematic diagram showing the set up for liquid phase epitaxial (LPE) growth of ferrite films. (b) Scanning electron microscopy(SEM) image of surface of a film of nickel zinc ferrite (NZFO) film grown on (111) MgO. (c) Energy dispersive spectroscopy data for NZFO film on (111) MgO. (d) X-ray diffraction data showing single crystal nature of NZFO grown on a (111) MgO substrate. Insets show the diffraction peaks from MgO and NZFO.

dipped into the melt for the isothermal growth for a predetermined period and raised slowly. The sample was then allowed to cool and the excess flux adhering to the films was removed by cleaning in warm 20% acetic acid. Since double-side polished substrates were used films grew on both sides of MgO. The growth rate was 0.2 – 0.7 μm/min, depending on T_g, and films with thicknesses in the range 2 -30 μm were grown.

2.1: Structural characterization of LPE films

A scanning electron microscope was used to examine the film quality and determine the chemical composition by energy dispersive x-ray spectroscopy (EDS). Films were found

to be free of defects as seen in the SEM image of Fig.1(b). The desired film composition was $Ni_{0.8}Zn_{0.2}Fe_2O_4$ whereas the measured composition was $Ni_{0.86}Zn_{0.14}Fe_2O_4$ which was slightly Ni rich and Zn deficient. A small amount of ZnO was then added to the melt (modified flux composition in Table 1) to compensate for the Zn-deficiency and the film grown with the modified flux had the composition $Ni_{0.85}Zn_{0.15}Fe_2O_4$ (Fig.1c). The film was found to have cubic spinel structure with lattice constant a_0 = 0.8357 nm and to be free of any impurity phases from X-ray diffraction data shown in Fig.1(d) for a film on (111) MgO. The data also confirm the single crystal nature of the NZFO film. It was, however, necessary to anneal the films at temperatures 800-900 °C to achieve the expected saturation magnetization as discussed next. Films were also grown on spinel $MgAl_2O_4$ substrates, but didn't produce good quality films and are not discussed here.

2.2: Magnetic Characterization of ferrite films

The ferrite films were characterized in terms of magnetic order parameters using a Faraday magnetic balance and a broad-band FMR system. Figure 2(a) shows magnetization *M* vs *H* data for a representative sample. The room-temperature data are for a 10.47 μm thick film on a 0.5 mm thick (111) MgO substrate and for in-plane *H*. A soft magnetic character with very low coercive field and a saturation magnetization $4\pi M_s$ = 3.4 ± 0.1 kG were measured for the sample. Upon annealing the film in air at 800-1000 °C, there was an increase in the magnetization value to $4\pi M_s$ = 3.6 ± 0.1 kG. All of the annealed films grown on (111) and (100) MgO substrates had $4\pi M_s \sim 3.6$ kG. The measurements reported here were made on composites with annealed ferrite films and $4\pi M_s$ values were in agreement with values reported for bulk and single crystal NiZn-ferrites [27].

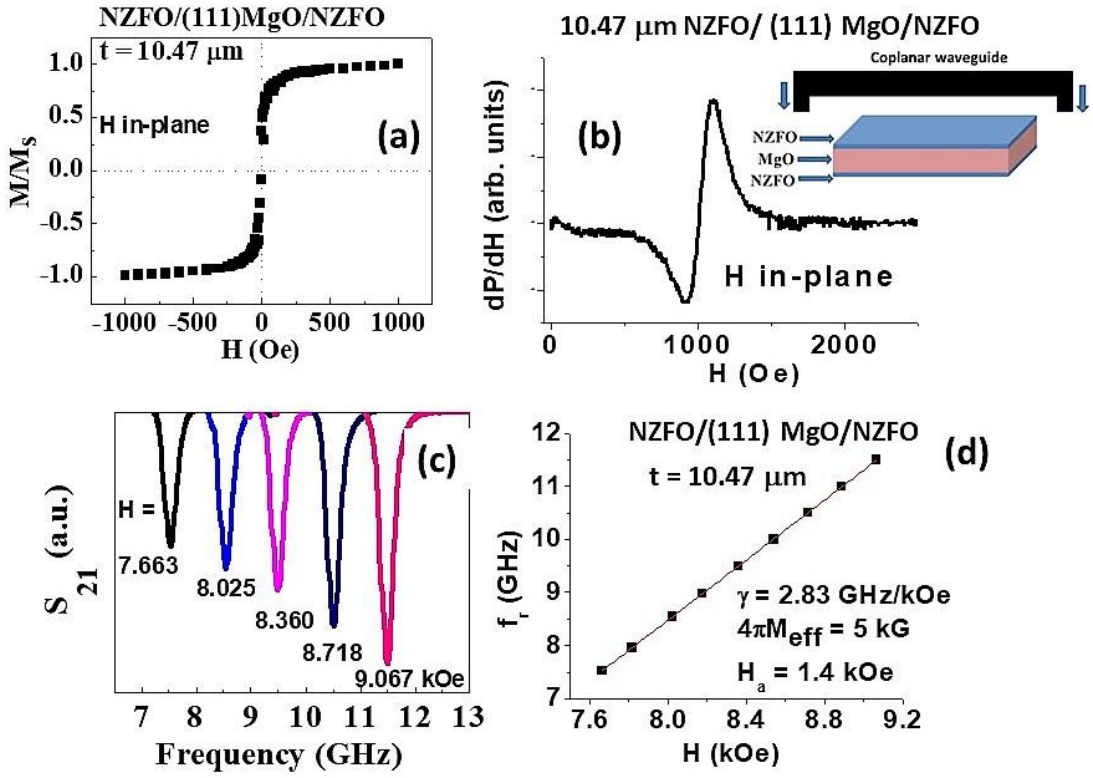

Fig.2

Fig.2. (a) Magnetization M vs H for 10.47 μm thick NZFO film on (111) MgO. The field H was parallel to the film plane. (b) Ferromagnetic resonance (FMR) profile of derivative of power absorbed at 7 GHz versus in-plane static field H for the NZFO film on (111) MgO. Inset shows the NZFO film on both sides of the substrate and the coplanar waveguide. The FMR absorption is due to the layer of NZFO in the proximity of microwave excitation structure. (c) Scattering matrix parameter S_{21} vs f as a function of H showing FMR for the 10.47 μm thick NZFO film on (111) MgO. The field H was applied perpendicular to the film plane. (d) Resonance frequency f_r as a function of H from data as in Fig.2(c) for the NZFO film on (111) MgO.

For FMR measurements the film was placed in a coplanar waveguide and excited with microwave power provided by a sweep generator or a vector network analyzer. Resonance profiles were obtained either by recording the derivative of the power absorbed, *dP/dH* vs *H* at constant frequency or by recording the profiles of scattering matrix S_{21} vs frequency *f* for constant *H*. Figures 2(b) and (c) show FMR profiles for a 10.47 μm thick

film of NZFO on both sides of (111) MgO for in-plane and out-of-plane H, respectively. The profiles are due to FMR in the ferrite layer in the proximity of the microwave magnetic field. The field-scan profile for f = 7 GHz in Fig.2(b) shows a symmetric FMR absorption with resonance field H_r ~ 1025 Oe and peak-to-peak line-width ΔH = 160 Oe. Our broad-band FMR system was used for determining both the gyromagnetic ratio γ, the effective saturation induction $4\pi M_{eff}$ and the anisotropy field H_a for the ferrite films. The S_{21} vs f data in Fig.2(c) for the 10.47 μm NZFO on (111) MgO were recorded for a series of H perpendicular to the samples plane and FMR is seen as absorption of microwave power. Figure 2(d) shows the resonance frequency f_r vs. H obtained from the profiles as in Fig.2(c) and f_r is related to H and magnetic parameters for the film by the expression

$$f_r = \gamma\ (H-4\pi M_{eff}) \qquad (1)$$

where $4\pi M_{eff} = 4\pi M_s + H_a$, and H_a is sum of magnetocrystalline and growth induced anisotropies. The γ-value determined from the slope of linear fit to the data in Fig.2 (d) is 2.83 GHz/kOe and $4\pi M_{eff}$= 5 kG. Using the value of $4\pi M_s$ = 3.6 kG from magnetization measurements, the estimated anisotropy field H_a = 1.4 kOe.

Similar FMR measurements were done on NZFO films of thickness t = 2-30 μm on (111) and (100) MgO substrates and estimated γ, $4\pi M_{eff}$ and H_a-values as a function of t are shown in Fig.3. For the films on (111) MgO γ-values are in the range 2.80-2.85 and do not show any systematic variation with film thickness whereas $4\pi M_{eff}$ increases from 4.8 kG to 5 kG as t is increased from 2 μm and to 7 μm and then levels off at this value for higher t. The in-plane anisotropy field H_a in Fig.3(b) for the NZFO films on (111) MgO ranges from 1.2 to 1.4 kOe. Films on (100) substrates, however, show a pronounced dependence of the

magnetic parameters on thickness with γ increasing from 2.8 GHz/kOe for t = 2 μm to 2.93 GHz/kOe for $t \geq 15$ μm and is accompanied by a decrease in $4\pi M_{eff}$ from 6.5 to 6.2 kG. The anisotropy is field H_a determined from $4\pi M_{eff}$ and $4\pi M_s$ and plotted in Fig.3(d) also decreases from 2.9 kOe for t = 2 μm to 2.6 kOe for t = 30 μm. The gyromagnetic ratio γ = 2.8 to 2.93 GHz/kOe for the LPE grown films are somewhat smaller than 3.0 reported for bulk polycrystalline and single crystal NiZn-ferrites [27]. The measured γ ~ 2.8 GHz/kOe corresponds to Lande g-factor g = 2.0 which is close to spin-only value and is smaller than g ~ 2.2 reported for bulk NiZn-ferrites [31].

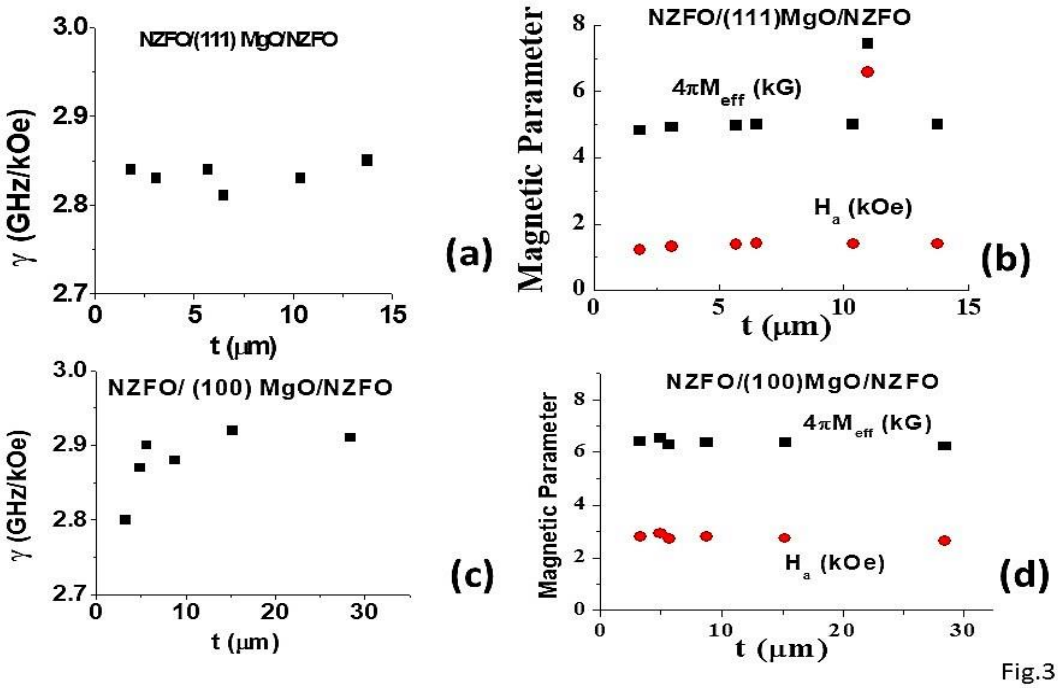

Fig.3.(a) Estimated values of the gyromagnetic γ and (b) $4\pi M_{eff}$ and in-plane anisotropy field H_a as a function of film thickness t for NZFO films on (111) MgO substrates. (c) and (d) show similar results for films of NZFO on (100) MgO.

A growth induced anisotropy field in the LPE films is evident from the magnetization and FMR measurements on the films grown on both (111) and (100) MgO substrates. The anisotropy field is easy-plane in nature for the LPE films and arises due the substrate-lattice

mismatch of 0.78% that leads to a tensile strain in the film. It is appropriate to compare the H_a values with reported values for similar thin film NiZn ferrites. In a recent study on pulsed laser deposition (PLD) of nickel ferrite films on (100) $MgAl_2O_4$, $MgGa_2O_4$ and $CoGa_2O4$ an easy-plane anisotropy H_a of 0.5 to 11.9 kOe was reported and attributed to a compressive strain on the film due to substrate-film lattice mismatch of 0.2 to 3.1% [32]. Similarly, very thin PLD films of NiZnAl-ferrite on $MgAl_2O_4$ were found to have an easy plane H_a of 10 kOe [33]. Thus our LPE films have magnetic parameters that are in general agreement with values reported for similar systems. We discuss next the use of these films in a composite with PZT for studies on converse ME effects.

3. Converse ME effects in composites of NiZn ferrite films on MgO and PZT

For studies on converse ME effects, ferrite films on MgO and polycrystalline PZT were used. Vendor supplied, pre-poled PZT (#850, American Piezo Ceramics) of dimensions 8 mm ×3 mm × 0.2 mm with silver electrodes was used. MgO substrate with NZFO films on both sides and of lateral dimensions 6 mm × 3 mm was bonded to PZT with an epoxy (ethyl cyanoacrylate). The thickness of the epoxy layer was measured to be 1 to 2 μm. Microwave measurements were carried out using a vector network analyzer (Agilent E8361A) with input power of -15 dBm. A standard electronic calibration was performed before measurements. The scattering parameter S_{21} vs f scans were recorded for FMR spectra under a constant bias field H perpendicular to the sample plane and for a series of H-values. This particular orientation of H will result in a linear shift in FMR frequency and is preferred over in-plane H. A dc voltage V = 0-500 V was applied across the thickness of PZT to generate E = 0 – 25 kV/cm. Samples of NZFO-(111) MgO-NZFO-PZT were

positioned in the coplanar waveguide as shown in Fig.4 so that the ferrite film was directly on top of the microwave excitation structure in order to achieve maximum absorption of microwave power under FMR. *The ferrite film between MgO and PZT does not give rise to any FMR signal and in the discussion to follow we represent the composites as NZFO/MgO/PZT.*

3.1: CME in composites of NZFO on (111) MgO and PZT

FMR measurements under an applied electric field were done on samples with ferrite film thickness ranging from 2 to 15 μm. Figure 4 shows S_{21} vs f for H = 8510 Oe and a series DC voltage V = 0-500 V applied across PZT for a sample with ferrite film with t =10.47 μm. The field E in this case was parallel to the poling field for PZT. For V=0, resonance with f_r = 8.945 GHz is seen in Fig.4 (b). With the application of V = 200 V, there is an up shift in f_r to 8.975 MHz and a further shift to 9.020 GHz for V = 500 V.

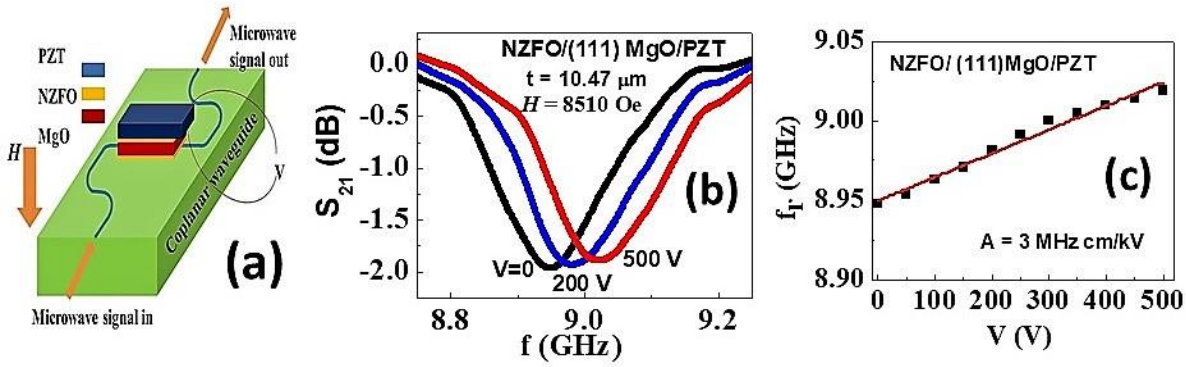

Fig.4. (a) Diagram showing the composite of NZFO/MgO/NZFO/PZT and the coplanar waveguide. The FMR signal is from the ferrite layer that is on top of the microwave excitation structure. The NZFO layer between MgO and PZT does not contribute to FMR and the composites are represented as NZFO/MgO/PZT. The electric field was applied with a voltage across PZT. (b) FMR in composites of 10.47 μm thick NZFO on 0.5 mm thick (111) MgO and 0.2 mm thick PZT for H perpendicular to sample plane. An upshift is seen in f_r with the application of E. (c) f_r vs V data obtained from profiles as in (b).

Figure 4(c) shows the dependence of f_r on V. Since the contribution to the resonance field due to piezoelectric strain in PZT is given by $H_{ME} = A\ E$, Kittel's equation can be written as [25,26]

$$f_r = \gamma\ (H\text{-}4\pi M_{eff} + A\ E) = \gamma\ (H\text{-}4\pi M_{eff} + AV/t\ ). \qquad (2)$$

One may, therefore, estimate the ME constant A from linear fit to the data as in Fig.4(b) and we estimated A = 3 MHz cm/kV for the composite. Similar measurements were done on composites with ferrite film thickness up to 15 μm and A-values were estimated from data as in Fig.4. Figure 5 shows the variation in A with t for the composites. A general decrease in A with increasing film thickness is seen with a maximum value of 5.6 MHz cm/kV and minimum of 2.5 MHz cm/kV. A detailed discussion on these results is provided in Sec.4.

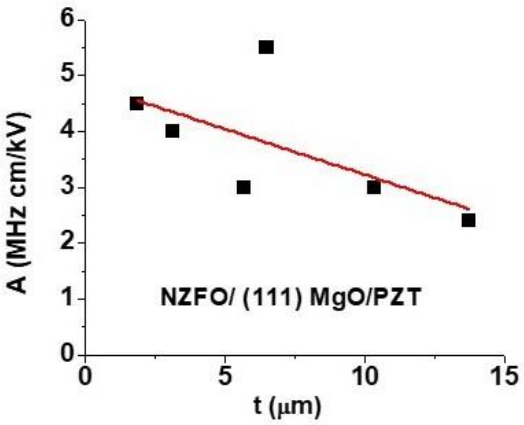

Fig.5

Fig.5. ME constant A versus ferrite film thickness t for composites of NZFO-(111)MgO-NZFO-PZT.

3.2 *CME in composites of NZFO-(100) MgO-NZFO-PZT*

Ferrite films with thickness 2 to 30 μm on (100) MgO were used for studies on CME in composites with PZT. Although films on 0.5 mm thick MgO were used for studies aimed at the dependence of A on t, we also grew a film on 0.2 mm MgO to study the influence of non-ferroic substrate on converse ME effects. Figure 6(a) shows FMR profiles for a representative sample 8.76 μm thick NZFO film on 0.5 mm thick (100) MgO and PZT. The

static field was applied perpendicular to the sample, along [100] direction of NZFO. For V=0 FMR occurs with f_r =10.85 GHz, the resonance frequency increases to 10.90 GHz upon the application of 150 V and then to 11 GHz for V=350 V. We estimated an ME constant A-value of 8.54 MHz cm/kV from the data on f_r vs V in Fig.6(b). The ferrite film thickness dependence of A-for NZFO/(100) MgO/PZT was obtained from data as in Fig.6 and is shown in Fig.7. A decrease in A, from 10 MHz cm/kV for t = 5 μm to 8 MHz cm/kV for t = 30 μm is seen. The overall strength of CME in the composites with NZFO films on 0.5 mm thick (100) MgO is at least a factor two or more stronger than in samples with NZFO films on 0.5 mm thick (111) MgO.

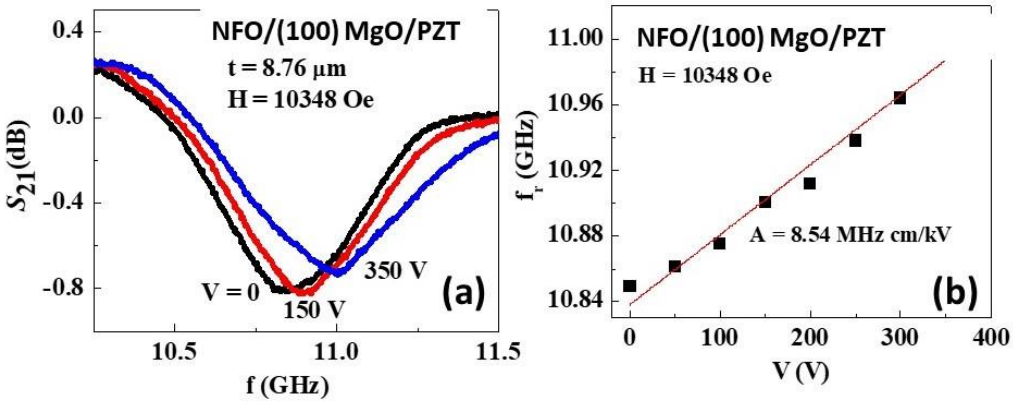

Fig.6. (a) FMR profiles for a series of voltages applied to composite of NZFO films on 0.5 mm thick (100) MgO substrate and PZT. (b) Resonance frequency f_r versus V for the composite.

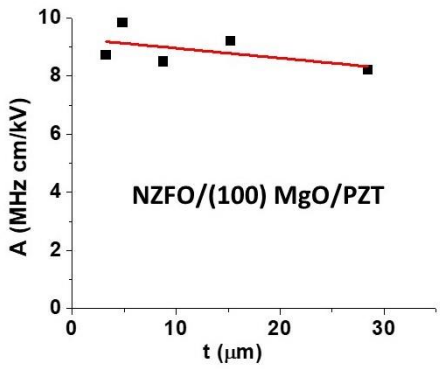

Fig.7. ME constant A versus ferrite film thickness t for composites of NZFO films on 0.5 mm thick (100) MgO and PZT.

The influence of a non-ferroic substrate, such as MgO, on the strength of the converse-ME effect has not been previously investigated. We grew NZFO films on 0.2 mm thick (100) MgO for studies aimed at addressing this particular aspect of the strain mediated coupling. Fig. 8 shows FMR profiles as a function of V applied to PZT in a composite with 20 μm thick ferrite on (100) MgO. The bias magnetic field H was perpendicular to the sample plane. The profiles in Fig. 8(a) show a *down-shift* in f_r when V = -150 V is applied to PZT.

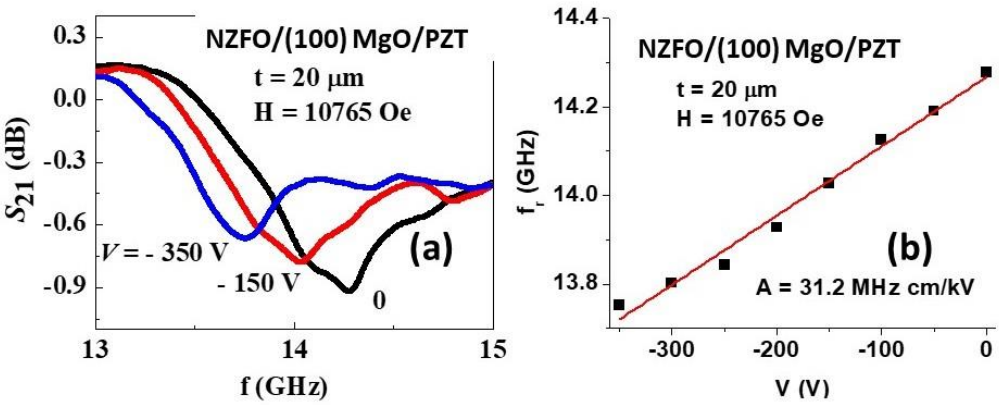

Fig.8. (a) FMR profiles as in Fig.6(a) for ferrite films on 0.2 mm thick (100) MgO substrate.(b) Resonance frequency f_r versus V for the bilayers.

In this case the voltage was applied in such a way that the electric field E was opposite to the poling field direction for PZT. A further reduction in f_r is observed when the magnitude of V is increased. The variation in f_r with V is linear as seen in the data of Fig. 8(b) and the ME constant A = 31.2 MHz cm/kV. Thus the reduction in the substrate thickness from 0.5 mm to 0.2 mm resulted in a factor of four increases in A. Next we discuss a model to understand the results on the dependence of A on the ferrite film and MgO substrate thicknesses shown in Figs. 4-8.

4. Theory

We consider a composite as in Fig.9 with a ferrite film of length L and thickness $t = {}^{m}t$ on a dielectric substrate with a thickness ${}^{s}t$ and mechanically coupled to a piezoelectric plate (PZT) with a thickness ${}^{p}t$. Since the second ferrite layer between MgO and PZT does not contribute to FMR absorption and its thickness is much smaller than MgO and PZT, it is not considered in the model and is not shown in Fig.9. The sample is in the *(1,2)* plane and the polarization *P* of PZT and static magnetic field *H* and electric field *E* are all in the direction *3*.

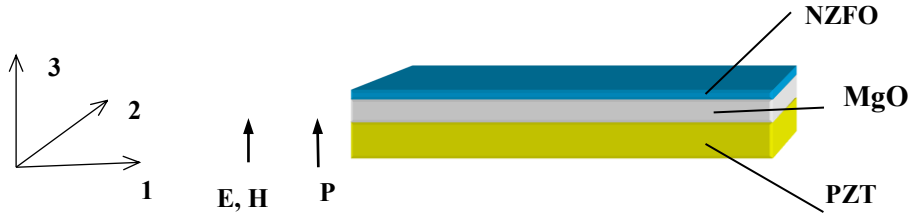

Fig.9. Schematic drawing of the composite structure consisting of a nickel zinc ferrite film (NZFO), substrate (MgO), and piezoelectric platelet (PZT) and the coordinate system assumed for the model. The NZFO layer between MgO and PZT is not shown. PZT is poled in direction 3 and bias field H and electric field E are also along the same direction.

If the direction of *E* is perpendicular to the plane of PZT then the thickness deformations ${}^{p}S_3$ due to the piezoelectric terms $d_{33}E_3$ and planar deformation ${}^{p}S_1$ due to $d_{31}E_3$ are present. Although from a mechanical point of view the structure has free surfaces and clamped interfaces, deformations along the thickness ${}^{p}S_3$, however, do not lead to deformation in the substrate and ferrite film. Since the PZT-MgO and MgO-NZFO interfaces are clamped, the displacement of PZT along the plane ${}^{p}S_1$ also leads to a displacement of the substrate ${}^{s}S_1$ and ferrite media ${}^{m}S_1$ (with p, s, and m denoting the parameters for piezoelectric layer, substrate and magnetic layer, respectively). These deformations along the plane, due to the Poisson effect, lead to deformations along the thickness of the sample.

Using this mechanism of deformation, we obtain the following equations for the components of the strain tensor:

$$ {}^{p}S_1 = \frac{1}{{}^{p}Y}({}^{p}T_1 - \nu\,{}^{p}T_2) + d_{31}E_3, \tag{3} $$

$$ {}^{p}S_2 = \frac{1}{{}^{p}Y}(-\nu\,{}^{p}T_1 + {}^{p}T_2) + d_{31}E_3, \tag{4} $$

$$ {}^{s}S_1 = \frac{1}{{}^{s}Y}({}^{s}T_1 - \nu\,{}^{s}T_2), \tag{5} $$

$$ {}^{s}S_2 = \frac{1}{{}^{s}Y}(-\nu\,{}^{s}T_1 + {}^{s}T_2), \tag{6} $$

$$ {}^{m}S_1 = \frac{1}{{}^{m}Y}({}^{m}T_1 - {}^{m}\nu\,{}^{m}T_2), \tag{7} $$

$$ {}^{m}S_2 = \frac{1}{{}^{m}Y}(-{}^{m}\nu\,{}^{m}T_1 + {}^{m}T_2), \tag{8} $$

where T denotes the component of stress tensors and ${}^{p}Y$, ${}^{s}Y$, ${}^{m}Y$ are Young's modules of PZT, MgO and NZFO. We assume that the Poisson ratio for piezoelectric, substrate and ferrite are equal, i.e. ${}^{p}\nu = {}^{s}\nu = {}^{m}\nu = \nu$. The condition of mechanical equilibrium gives the following equations:

$$ {}^{m}T_1\,{}^{m}t + {}^{s}T_1\,{}^{s}t + {}^{p}T_1\,{}^{p}t = 0, \tag{9} $$

$$ {}^{m}T_2\,{}^{m}t + {}^{s}T_2\,{}^{s}t + {}^{p}T_2\,{}^{p}t = 0 \tag{10} $$

Proceeding from the condition of a continuous medium and using the fact that the layers are thin, we can assume that the in-plane displacements u of the layers are the same, i.e. ${}^{p}u_1 = {}^{s}u_1 = {}^{m}u_1 = u_1$ and ${}^{p}u_2 = {}^{s}u_2 = {}^{m}u_2 = u_2$. With these assumptions and using the equilibrium conditions in Eq. (9) and Eq. (10) we get the following expressions for the strain S_1 and S_2:

$$ S_1 = S_2 = \frac{{}^{p}t\,{}^{p}Y d_{31}E_3}{({}^{p}t\,{}^{p}Y + {}^{s}t\,{}^{s}Y + {}^{m}t\,{}^{m}Y)} = \frac{{}^{p}Y}{\bar{Y}} \cdot \frac{{}^{p}t}{({}^{p}t + {}^{s}t + {}^{m}t)} \cdot d_{31}E_3, \tag{11} $$

where $\bar{Y} = \dfrac{({}^{p}t\,{}^{p}Y + {}^{s}t\,{}^{s}Y + {}^{m}t\,{}^{m}Y)}{({}^{p}t + {}^{s}t + {}^{m}t)}$ is the average value of Young's module of the structure.

The equation of motion of magnetization has the following form:

$$\frac{\partial \vec{M}}{\partial t} = \gamma[\vec{M}, \vec{H}_{eff}], \qquad (12)$$

where γ is the gyromagnetic ratio, $\vec{M}$ and $\vec{H}_{eff}$ are magnetization and effective magnetic field. The effective magnetic field $\vec{H}_{eff}$ is the sum of the external magnetic field $H = \vec{H}_0$, the magnetocrystalline anisotropy $\vec{H}_a$, the shape anisotropy $\vec{H}_f$ and magneto-electric (or magnetoelastic anisotropy) $H_{ME} = \vec{H}_{el}$. The magnetoelastic anisotropy under the action of the mechanical stress, according Ref. [34], when $H_a << H_0$, can be written in the form:

$$H_{el} = \frac{3^m T}{2M_s}(\lambda_{100} - \frac{3}{2}(\lambda_{100} - \lambda_{111})\sin^2\theta), \qquad (13)$$

where M_s is saturation magnetization, θ is the angle between H_0 and the [100] direction, and λ_{100} and λ_{111} are magnetostriction constants. Using the Poisson ratio, the Boltzmann superposition principle and Eq. (11) we obtained the following expression for the shift of the resonance:

$$\Delta\omega = \gamma \frac{3^m Y}{M_s} \frac{^p Y}{\bar{Y}} \frac{^p t}{(^p t + {}^s t + {}^m t)}(\lambda_{100} - \frac{3}{2}(\lambda_{100} - \lambda_{111})\sin^2\theta)\nu d_{31} E_3. \qquad (14)$$

As can be seen from Eq. (14) the shift of the resonance line has linear dependence on E and $\Delta\omega = AE$ and the converse magnetoelectric coefficient A is given by

$$A = \gamma \frac{3^m Y}{M_s} \frac{^p Y}{\bar{Y}} \frac{^p t}{(^p t + {}^s t + {}^m t)}(\lambda_{100} - \frac{3}{2}(\lambda_{100} - \lambda_{111})\sin^2\theta)\nu d_{31}. \qquad (15)$$

As can be seen from Eq. (14) the shift of the resonance line decreases with increasing ferrite and substrate thickness. Since the thickness of the substrate $^s t$ is comparable to the thickness of PZT $^p t$, and the thickness of the ferrite $^m t$ is much smaller than $^s t$, the dependence of the shift of the line on $^s t$ is stronger than the dependence on ferrite film thickness. For the case $^m t << {}^p t + {}^s t$ we have

$$\frac{{}^{p}t}{({}^{p}t+{}^{s}t+{}^{m}t)} \approx \frac{{}^{p}t}{({}^{p}t+{}^{s}t)}(1-\frac{{}^{m}t}{({}^{p}t+{}^{s}t)}), \tag{16}$$

and for the ME constant A we get the following expression

$$A \approx \gamma \frac{3{}^{m}Y}{M_s}\frac{{}^{p}Y}{\bar{Y}}(\lambda_{100}-\frac{3}{2}(\lambda_{100}-\lambda_{111})\sin^2\theta)\nu d_{31}\frac{{}^{p}t}{({}^{p}t+{}^{s}t)}(1-\frac{{}^{m}t}{({}^{p}t+{}^{s}t)})) = C(1-k\cdot{}^{m}t), \tag{17}$$

where $C = \gamma \frac{3{}^{m}Y}{M_s}\frac{{}^{p}Y}{\bar{Y}}(\lambda_{100}-\frac{3}{2}(\lambda_{100}-\lambda_{111})\sin^2\theta)\nu d_{31}\frac{{}^{p}t}{({}^{p}t+{}^{s}t)}$, $k = \frac{1}{({}^{p}t+{}^{s}t)}$. (18)

Thus, the line shift in the resonance line decreases linearly with increasing ferrite thickness, in agreement with the data in Fig. 5 and Fig.7). For numerical calculations we use the following parameters [25, 35]:

PZT:

$$\begin{aligned} &{}^{p}c_{11} = 12.6\times10^{10}\,N/m^2, \quad {}^{p}c_{12} = 7.95\times10^{10}\,N/m^2, \\ &{}^{p}c_{13} = 8.4\times10^{10}\,N/m^2, \quad {}^{p}c_{33} = 11.7\times10^{10}\,N/m^2, \quad d_{31} = -175\times10^{-12}\ m/V; \end{aligned}$$

NZFO:

$$\begin{aligned} &{}^{m}c_{11} = 21.99\times10^{10}\,N/m^2, \quad {}^{m}c_{12} = 10.94\times10^{10}\,N/m^2, \\ &{}^{m}c_{44} = 8.12\times10^{10}\,N/m^2, \quad \lambda_{111} = -20.7\times10^{-6}, \quad \lambda_{100} = -30\times10^{-6}; \end{aligned} \tag{19}$$

MgO:

$$\begin{aligned} &{}^{s}c_{11} = 28.6\times10^{10}\,N/m^2, \quad {}^{s}c_{12} = 8.7\times10^{10}\,N/m^2, \\ &{}^{s}c_{44} = 14.8\times10^{10}\,N/m^2. \end{aligned}$$

The components of the compliance tensor are expressed in terms of the components of the elasticity tensor by means of relations: $\overleftrightarrow{s} = (\overleftrightarrow{c})^{-1}$ and the Young's modulus is determined by $Y = \frac{1}{s_{11}}$. In the transformation of the coordinate system, the components of the compliance tensor change according to relation

$$s_{i'j'k'l'} = \beta_{i'i}\beta_{j'j}\beta_{k'k}\beta_{l'l}s_{ijkl}, \tag{20}$$

where β is direction cosine matrix for the axes 1′, 2′, 3′ about the crystallographic axes 1, 2, 3.

Using these relations we can calculate the ME constant A for the other orientations of substrate and ferrite.

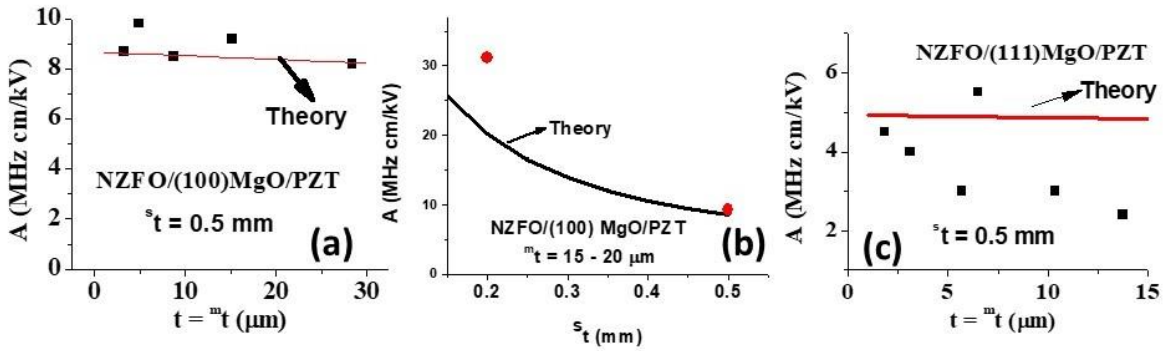

Fig.10: (a) Theoretical A values as a function of ferrite film thickness for composites of NZFO/ 0.5 mm thick (100) MgO and PZT. Measured A values (filled squares) are shown for comparison. (b) Theoretical values of A vs thickness of (100) MgO substrate for composites of NZFO/MgO and PZT. Measured A values (filled circles) are shown for comparison. (c) Results as in (a) for composites of NZFO/(111) MgO and PZT. Measured values of A (filled squares) are shown for comparison. Measured A values are from data in Figs. 5, 7 and 8.

Figure 10 shows the calculated values of the ME constant A for the composites. Results for NZFO/(100) MgO/PZT are shown in Figs. 10 (a) and (b). For these calculations we used $4\pi M_s = 3.6\ kG$, $^{p}t = 0.2\ mm$, and the values of elastic modules given in Eq.(19). Estimated A-values in Fig.10(a) for ^{s}t = 0.5 mm predict a decrease in A from 8.7 MHz cm/kV for ^{m}t = 1 μm to 8.3 MHz cm/kV for ^{m}t = 30 μm and are in very good agreement with measured A-values (from Fig.5). The model predicts a significant dependence of A on the substrate thickness as shown in Fig.10 (b). One anticipates an increase in A, from 8.5 to 34.5 MHz cm/kV when the substrate thickness is decreased from 0.5 to 0.1 mm and A-values are in general agreement with measured values for ^{s}t = 0.2 mm and 0.5 mm.

For samples of NZFO/(111)MgO/PZT the transformations in Eq.(20) were used to calculate A and its dependence on film thickness is shown in Fig.10(c). We obtained

$A = 4.86\ MHz\ cm/kV$ for ^{m}t = 1 μm and it decreases to 4.7 MHz cm/kV for ^{m}t = 15 μm. The measured *A*-values, however, show almost 50% decrease for the same variation in the film thickness. There is overall general agreement between theory and data in Fig.10. Any difference between the theoretical and experimental values could be due to the use of bulk single crystal parameters (magnetostriction and elastic constants) for ferrites. The key inference from results in Fig.10 is that a composite of a ferroelectric and a thick ferrite film on a thin substrate will have strong converse ME interactions.

5. Discussion

It is clear from the results of our studies that growth of nickel zinc ferrite films by LPE yielded films with a wide variation in thickness, 2 to 30 μm, suitable for investigations on converse ME effects. Such a range in thickness is essential for studies aimed at the dependence of the strength of ME coupling on volume/thickness for the ferroic phases. Liquid phase epitaxy had to be utilized since growth by techniques such as PLD, molecular beam epitaxy or chemical vapor deposition (CVD) are not viable options for growing thick films. Substrates of MgO with 0.78% lattice mismatch with NZFO films were selected since films cannot be grown by LPE on substrates with a large lattice mismatch. Magnetization and FMR measurements yielded magnetic order parameters for the films that were in agreement with values reported for bulk single crystal ferrites. The growth induced tensile strain on the films was the cause of easy plane anisotropy in the films on both (111) and (100) MgO. The films on (100) MgO, however, showed a much higher anisotropy field H_a than for (111) MgO. A decrease in H_a with increasing film thickness was evident from the data in films on both substrates.

For studies on ME effects composites of ferrite films were made with PZT of identical dimensions and ferroelectric parameters so that any variation in the ME interactions could be understood in terms of variations in the magnetic properties of the ferrite films. Ferromagnetic resonance measurements under E were made for static field H perpendicular to the sample plane since the E-induced shift in the resonance field is a linear term, AE, in the Kittel's equation (Eq.1) and the ME constant could be determined directly from data on f_r vs E. Results in Figs. 5-8 on the strength of ME coupling indicate strong interactions with A values showing a nearly 100% enhancement when the thickness of NZFO on (111) MgO is decreased from 15 μm to 2 μm. Samples with films on (100) MgO have a much stronger interaction than those on (111) MgO with the A-value showing a linear decrease with increasing film thickness. A model for converse ME effect that takes into account the influence of non-ferroic substrate was developed and estimates of coupling strength as a function of film and substrate thicknesses are in agreement with the data.

Past reports on CME in similar composites include 1 μm thick nickel ferrite films directly deposited onto 0.5 mm thick lead magnesium niobate-lead titanate (PMN-PT) or lead zinc niobate-lead titanate (PZN-PT) [17]. Measurements of CME by FMR and M vs H under E yielded A values of 45-66 MHz cm/kV and the higher value compared to the present system is due to relatively small ferrite film thickness, absence of a non-ferroic substrate and thicker ferroelectric phase with a much higher d-value compared to PZT. Converse ME effects was also investigated in epoxy bonded composites of YIG film on GGG substrates and PZT or PMN-PT and the measured A ~ 2 MHz cm/kV is smaller than

the values for the systems studied in this work [16,21]. The ME coefficient reported in this study is a factor of 4-16 higher than for hexagonal ferrite-PZT bilayers [22,24].

Finally, the *E*-tuning of FMR technique utilized for the determination of the strength of CME also has technological importance [18-21, 24]. Ferrites, due to low losses at high-frequencies, are used in FMR-based microwave devices such as resonators and filters. Tuning the operating frequency of the device, however, requires a source of variable magnetic field such as a solenoid. The magnetic field tuning in general is slow, noisy and requires a large power for operation. An attractive alternative to *H*-tuning is the *E*-tuning that can be achieved by replacing the ferrite with a ferrite-ferroelectric composite. The tuning of the device with a voltage applied to the ferroelectric layer will be fast and passive and will facilitate miniaturization and integration with semiconductor devices. A key figure of merit for the device is the tuning band width compared to FMR line-width. Figure 11 shows the FMR line-width ΔH vs frequency f for NZFO films grown on (111) and (100) MgO substrates. The film grown on (100) MgO has a ΔH of ~ 80 Oe. The corresponding

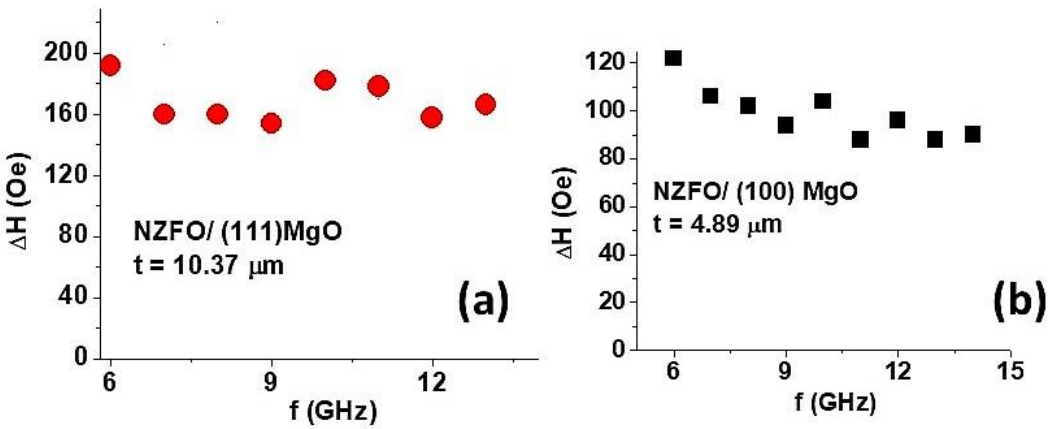

Fig.11. Representative FMR linewidth ΔH as a function of frequency for LPE grown NZFO films on 0.5 mm thick (a) (111) MgO and (b) (100) MgO substrates.

frequency width is 224 MHz and is much smaller than the ΔH for films on (111) MgO. Thus film of NZFO on 0.1 – 0.2 mm thick (100) MgO substrates have the potential for use in a composite with PZT or PMN-PT for broad-band microwave devices.

6. Conclusions

The strain mediated converse magneto-electric coupling has been investigated in composites of PZT and single crystal nickel zinc ferrite films on MgO substrates. Epitaxial NZFO films of thickness 2-30 μm were grown on MgO (100) and (111) substrates by liquid phase epitaxy. The films were characterized in terms of magnetic order parameters and were found to have growth induced in-plane anisotropy filed H_a that is larger in films on (100) MgO than for films on (111) MgO. The films were bonded to PZT and FMR was measured with the static magnetic field and electric field perpendicular to the sample plane. The strength A of CME was obtained from data on E-induced shift in the FMR frequency and it ranged from 2.5 to 31.2 MHz cm/kV, depending on the ferrite film orientation and substrate thickness. Composites with (100) ferrite films showed a factor of 2 to 4 stronger ME coupling than for (111) films. A substantial increase in A, from 8 to 31 MHz cm/kV, was measured when the substrate thickness was decreased from 0.5 to 0.2 mm. A theoretical model was developed and the influence of MgO substrate that did not contribute to the ME coupling was considered. Estimates of A were obtained as a function of film thickness and orientation and substrate thickness were obtained and found to be in good agreement with the data.

Acknowledgments

The research at Oakland University was supported by grants from the National Science Foundation (ECCS-1307714, DMR-1808892). The efforts at Hubei University was supported by the National Science Foundation of China (Grant Nos. 51372074, 51472078). The research at AFRL was supported by the Air Force Office of Scientific Research under project number FA9550-15RXCOR198 and a Summer Faculty Fellowship for G.S.

References

1. Ce-Wen Nan, M. I. Bichurin, S. Dong, D. Viehland, and G. Srinivasan, J. Appl. Phys. **103**, 031101 (2008).
2. Dwight Viehland,Jie Fang Li,Yaodong Yang, Tommaso Costanzo, Amin Yourdkhani, Gabriel Caruntu,Peng Zhou, Tianjin Zhang, Tianqian Li,Arunava Gupta,Maksym Popov, Gopalan Srinivasan, J. Appl. Phys. **124**, 061101 (2018).
3. M. M. Vopson, Critical Reviews in Solid State and Materials Sciences **40**, 223 (2015).
4. Z. Chu, M. PourhosseiniAsl, and S. Dong, Journal of Physics D: Applied Physics, 51, 243001 (2018).
5. Composite Magnetoelectrics: Materials, Structures, and Applications, Eds: G. Srinivasan, S. Priya, and N. X. Sun, Woodhead Publishing Series in Electronic and Optical Materials, No.62, 2015.
6. J. Van Suchtelen, Philips Res. Rep. **27**, 28 (1972).
7. J. Fukushima, K. Ara, T. Nojima, S. Iguchi, Y. Hayashi, and H. Takizawa, Applied Physics Letters **112**, 212903 (2018).
8. M. Gao, Ravindranath Viswan, Xiao Tang, Chung Ming Leung, Jiefang Li, and D. Viehland. Scientific reports **8**, 323 (2018): 323.
9. Y. Yan, Yuan Zhou, and Shashank Priya, Applied Physics Letters **104**, 032911 (2014).
10. J. Cui, Cheng-Yen Liang, Elizabeth A. Paisley, Abdon Sepulveda, Jon F. Ihlefeld, Gregory P. Carman, and Christopher S. Lynch, Applied Physics Letters **107**, 092903 (2015).
11. M. Zhu, Tianxiang Nan, Bin Peng, Yijun Zhang, Ziyao Zhou, Xi Yang, Wei Ren, Nian X.

Sun, and Ming Liu, IEEE Transactions on Magnetics **53**, 1 (2017).

12. P. Hayes, V. Schell, S. Salzer, D. Burdin, E. Yarar, A. Piorra, R. Knöchel, Y. K. Fetisov, and E. Quandt. Journal of Physics D: Applied Physics **51**, 354002 (2018).
13. A. McDannald, Linghan Ye, Claudia Cantoni, Sreenivasulu Gollapudi, Gopalan Srinivasan, Bryan D. Huey, and Menka Jain, Nanoscale **9**, 3246 (2017).
14. G. Sreenivasulu, H. Qu, and G. Srinivasan. Materials Science and Technology **30**, 1625 (2014).
15. M. M. Vopson, E. Zemaityte, M. Spreitzer, and Esmaeil Namvar. Journal of Applied Physics **116**, 113910 (2014).
16. S. Shastry, G. Srinivasan, M. I. Bichurin, V. M. Petrov, and A. S. Tatarenko, Phys. Rev. B. **70**, 064416 (2004).
17. N. Li, Ming Liu, Ziyao Zhou, Nian X. Sun, D. V. B. Murthy, Gopalan Srinivasan, Tonya M. Klein, Vladimir M. Petrov, and Arunava Gupta. Applied Physics Letters **99**, 192502 (2011).
18. J. Lou, Ming Liu, David Reed, Yuhang Ren, and Nian X. Sun. Advanced Materials **21**, 4711 (2009).
19. J. Das, Young-Yeal Song, Nan Mo, Pavol Krivosik, and Carl E. Patton. Advanced Materials **21**, 2045 (2009).
20. J. H. Leach, H. Liu, V. Avrutin, E. Rowe, Ü. Özgür, H. Morkoc, Y-Y. Song, and M. Wu. Journal of Applied Physics **108**, 064106 (2010).
21. Y. K. Fetisov and G. Srinivasan, Applied physics letters **88**, 143503 (2006).
22. G. Srinivasan, I. V. Zavislyak, and A. S. Tatarenko, Appl. Phys. Lett. **89**, 152508

(2006).

23. J. Lian, Freddy Ponchel, Nicolas Tiercelin, Ying Chen, Denis Rémiens, Tuami Lasri, Genshui Wang, Philippe Pernod, Wenbin Zhang, and Xianlin Dong. Applied Physics Letters **112**, 162904 (2018).
24. N. X. Sun and G. Srinivasan, SPIN **2**, 1240004 (2012).
25. M. I. Bichurin, I. A. Kornev, V. M. Petrov, A. S. Tatarenko, Yu. V. Kiliba, and G. Srinivasan, Phys. Rev. B **64**, 094409 (2001).
26. M. I. Bichurin, V. M. Petrov, Yu. V. Kiliba, and G. Srinivasan, Phys. Rev. B. **66**, 134404 (2002).
27. Landolt-Bornstein; Numerical data and functional relationships in science and technology, Group III, Crystal and Solid State Physics, vol 4(b), Magnetic and Other Properties of Oxides, eds. K.-H. Hellwege and A. M. Springer, Springer-Verlag, New York (1970).
28. H. L. Glass and M. T. Elliot. Journal of Crystal Growth **34**, 285 (1976).
29. F. S. Stearns and H. L. Glass. Materials Research Bulletin **11**, 1319 (1976).
30. J. M. Robertson, M. Jansen, B. Hoekstra, and P. F. Bongers. Journal of Crystal Growth **41**, 29 (1977).
31. W. H. Von Aulock, Handbook of Microwave Ferrite Materials, Academic, New York 1963.
32. A. V. Singh, Amit V., Behrouz Khodadadi, Jamileh Beik Mohammadi, Sahar Keshavarz, Tim Mewes, Devendra Singh Negi, Ranjan Datta, Zbigniew Galazka, Reinhard Uecker, and Arunava Gupta. Advanced Materials 29, 1701222 (2017).

33. S. Emori, Benjamin A. Gray, Hyung-Min Jeon, Joseph Peoples, Maxwell Schmitt, Krishnamurthy Mahalingam, Madelyn Hill et al. Advanced Materials **29**, 1701130 (2017).

34. G. A. Petrakovsii and E. M. Smokotin, Sov. Phys. JETP **28**, 1101 (1969).

35. M.A. Durand, Phys. Rev. **50**, 449, (1936).